Planetary and Space Science 61 (2012) 161–167

Contents lists available at ScienceDirect

Planetary and Space Science

journal homepage: www.elsevier.com/locate/pss

Recovery and characterization of Neptune's near-polar stratospheric hot spot

Glenn S. Orton [a,*], Leigh N. Fletcher [b], Junjun Liu [c], Tapio Schneider [c], Padma A. Yanamandra-Fisher [a], Imke de Pater [d], Michelle Edwards [e], Thomas R. Geballe [f], Heidi B. Hammel [g], Takuya Fujiyoshi [h], Therese Encrenaz [i], Eric Pantin [j], Olivier Mousis [k], Tetsuharu Fuse [l]

[a] MS 169-237, Jet Propulsion Laboratory, California Institute of Technology, 4800 Oak Grove Drive, Pasadena, CA 91109, USA
[b] Atmospheric, Oceanic and Planetary Physics, Clarendon Laboratory, University of Oxford, Parks Road, Oxford OX1 3PU, United Kingdom
[c] California Institute of Technology, Pasadena, CA 91125, USA
[d] Astronomy Department, 601 Campbell Hall, University of California, Berkeley, CA 94720-3411, USA
[e] Gemini Observatory, Colina El Pino via s/n Casilla 603, La Serena, Chile
[f] Gemini Observatory, 670N. A'ohoku Place, Hilo, HI 96720, USA
[g] Space Science Institute, 72 Sarah Bishop Road, Ridgefield, CT 06877, USA
[h] Subaru Telescope, 650N. A'ohoku Place, Hilo, HI 96720, USA
[i] LESIA, Observatoire de Paris, F-92195, Meudon, France
[j] Centre d'Etudes Atomiques, Saclay, 91190 Gif-sur-Yvette, France
[k] Institut UTINAM, CNRS-UMR 6213, Observatoire des Sciences de l'Univers THETA, Université de Franche-Comté, CP 1615, 25010, Besançon Cedex, France
[l] Kashima Space Research Center, National Institute of Information and Communications Technology, Ibaraki 314-8501, Japan

ARTICLE INFO

Article history:
Received 4 December 2010
Received in revised form
15 June 2011
Accepted 18 June 2011
Available online 30 June 2011

Keywords:
Neptune
Stratosphere
Temperature
Dynamics
Radiative heating

ABSTRACT

Images of Neptune obtained in 2006 at ESO's Very Large Telescope (Orton et al., 2007, Astronomy & Astrophysics 473, L5) revealed a near-polar hot spot near 70°S latitude that was detectable in filters sampling both stratospheric methane (7 μm) and ethane (~12 μm) emission. Such a feature was not present in 2003 Keck and 2005 Gemini North observations, which showed only a general warming trend toward Neptune's pole that was longitudinally homogeneous. Because of the paucity of longitudinal sampling in the 2003, 2005 and 2006 images, it was not clear whether the failure to see this phenomenon in 2003 and 2005 was simply the result of insufficient longitudinal sampling or whether the phenomenon was truly variable in time. To unravel these two possibilities, we made follow-up observations on large telescopes that were capable of resolving Neptune at thermal-infrared wavelengths: Gemini South in 2007 and 2010 using the T-ReCS instrument, Subaru in 2008 using the COMICS instrument and VLT in 2008 and 2009 using the VISIR instrument. Two serendipitous T-ReCS images of Neptune were also obtained in 2007 using a broad N-band (8–14 μm) filter, whose radiance is dominated by stratospheric emission from both methane and ethane. The feature was recovered (i) in 2007 with T-ReCS in the broad N-band image and (ii) in 2008 with COMICS in a 12.5-μm image. However, T-ReCS observations in 2010 that covered up to 250° of longitude did not show evidence of an off-polar hot spot. Although we have not definitively ruled out the possibility that various observers have simply missed a semi-permanent feature, it seems statistically very unlikely to be the case. With only 3 sightings in 13 independent observing epochs, it is likely that the phenomenon is ephemeral in time. A possible origin for the phenomenon is a large planetary wave that is dynamically confined to the high-latitude regions characterized by prograde zonal winds. It may be episodically excited by dynamical activity deeper in the atmosphere. This must be coupled with mixing near the poles that destroys or at least substantially attenuates the hot spot over the south pole that leads to an appearance of the typical polar stratospheric hot spot being offset in latitude.

1. Introduction

Initial observations of spatially resolved thermal emission from Neptune's stratosphere showed a general enhancement at its south pole. This was not unexpected because the inclination of Neptune's rotational axis to the ecliptic makes its atmosphere subject to substantial seasonal warming and cooling. This is

* Corresponding author. Tel.: +1-818-354-2460; fax: +1-818-393-4619.
E-mail addresses: Glenn.Orton@jpl.nasa.gov, go@scn.jpl.nasa.gov (G.S. Orton).

0032-0633/$ - see front matter © 2011 Elsevier Ltd. All rights reserved.
doi:10.1016/j.pss.2011.06.013

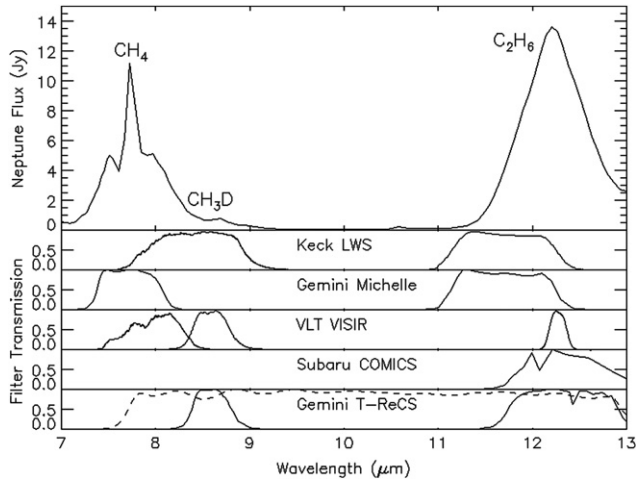

Fig. 1. Spitzer Infrared Spectrometer (IRS) spectrum of Neptune (top panel), plotted against normalized transmission functions of filters used in this study (bottom panels). Except for the N-band T-ReCS filter (shown as dashed line), wavelengths were chosen specifically to sample emission from stratospheric methane, deuterated methane and ethane. The influence of telluric emission is not accounted for in the plot of the spectrum of Neptune (top panel). The flux from the CH_4 7.7-μm feature is substantially attenuated by the absorption by telluric water vapor and methane. Thus, the easiest wavelengths to detect stratospheric emission are those associated with the 12.2-μm ethane feature. The approximate range of pressures in Neptune's atmosphere of peak emission detected in the 7.7-μm filter is 0.2–0.5 mbar, in the 8.7-μm filter it is 1–2 mbar, and in the 12.2-μm filter it is 1.5–3 mbar.

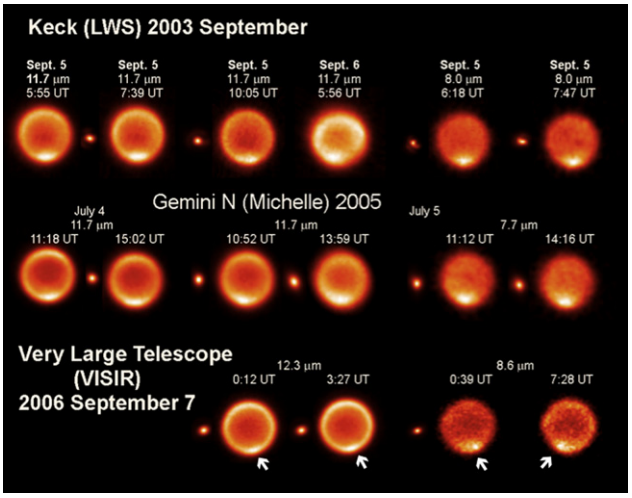

Fig. 2. Images of stratospheric emission from Neptune in 2003 from the W. M. Keck Telescope reported by Martin et al. (2006, 2008), in 2005 from the Gemini North Telescope, reported by Hammel et al. (2007), and in 2006 from the Very Large Telescope (UT3, "Melipal"), reported by Orton et al. (2007). The instrument used is denoted in parentheses. The date and time at the mid-point of each image acquisition are noted, as is the central wavelength of each filter. The quality of resolution of features on the disk can be judged by a point-spread function for standard stars that were observed closest to the Neptune observations at the same wavelength. Where available, these are displayed alongside each image: γ Aql (HD 199345) for the "early" Keck LWS observations and HD 199345 for the "late" observations in 2003; HD 199345 for all the Gemini North observations in 2005; and HD200914 for the "early" VLT VISIR observations and HD200514 for the observation at 3:27 UT (no stellar image was taken near the time of the image at 7:28 UT). The 12.4 h period of the neutral atmosphere at the is in near-cadence with the longitudes available on several sequential nights; thus it is likely that observations from Gemini North on 5 July 2005, sampled nearly the same atmospheric features at 70°S as on the previous night. The 2006 discovery detection is indicated with arrows, where the regular polar hot spot appears to be replaced by an off-polar feature, which has rotated behind the planet and was detected on the opposite limb ~7 h later. In retrospect, we note a possible offset associated with the 11.7 μm observation on 4 July 2005, taken at 11:18 UTC.

particularly true in its stratosphere, where the energy budget is not dominated by convective transport, as it is in the deeper atmosphere. Thus, substantial stratospheric warming was expected at Neptune's south pole, which has been under continuous exposure to sunlight for over 70 years. Saturn, which is similarly subject to seasonal forcing, has enhanced polar emission, detected as early as 1973 (Gillett and Orton, 1975), and mapped in detail from the ground (Orton and Yanamandra-Fisher, 2005) and by the Cassini spacecraft (Fletcher et al., 2008). The mid-infrared spectra of both planets is dominated by stratospheric emission from methane (CH_4) near 7–8 μm and ethane (C_2H_6) near 11–13 μm (Fig. 1, top panel). Enhanced emission was detected at Neptune's south pole both from stratospheric methane and ethane in images taken by the Keck LWS in 2003 (Martin et al., 2006, 2008), as well as by the Gemini North Michelle instrument in 2005 (Hammel et al., 2007), as shown in Fig. 2. The filters used for these and the new images we present here are illustrated in the bottom panels of Fig. 1. Orton et al. (2007) also found Neptune's upper troposphere to be warm, from observations made at longer wavelengths; here we confine our discussion to the stratosphere.

The 2006 detection by Orton et al. (2007) of a compact region of enhanced stratospheric emission near 70°S (planetocentric) latitude was unexpected. These data were taken from ESO's very large telescope using the VISIR mid-infrared camera/spectrometer (Fig. 2). A compact region of enhanced radiance was detected in both ethane and methane emission, and observed rotating completely around the planet in images of methane emission (Fig. 2, third row of images). Its rotation period of 12.4 ± 1.0 h (correcting an error made by Orton et al., who cited a value of 13.8 ± 1.0 h) was consistent with the ~12 h period associated with the neutral atmosphere at this latitude at cloud-top levels (Fig. 3), and not with the 16 h rotation rate of Neptune's magnetic field. This fact argued against the feature being auroral in origin.

In an effort to shed some light on the origin of this phenomenon in the neutral atmosphere, we sought additional observations to determine whether (i) the enhancement is a semi-permanent phenomenon that was simply missed in 2003 and 2005 because of incomplete longitudinal sampling, or (ii) the phenomenon is genuinely ephemeral. We proposed further observations to pursue this question and were granted time on various 8-m telescopes, whose diffraction-limited resolution allows us to resolve thermal emission from Neptune's disk.

2. Data acquisition and reduction

Images were acquired at several observatories over the period between 2007 and 2010. Standard procedures were used for mid-infrared image acquisition and reduction for both the 2003–2006 (Fig. 2) and 2007–2010 (Fig. 4) data. The latter were taken with several mid-infrared facility instruments at 8 m-class telescopes: T-ReCS (Telesco et al., 1998; de Buizer and Fisher, 2005) at the Gemini South Telescope in service time, COMICS (Kataza et al., 2000) at the Subaru Telescope in classical time, and VISIR (Lagage et al., 2000) at ESO's Very Large Telescope in service time.

Rapid-frequency oscillation ("chopping") of the secondary mirror of each telescope was performed between two positions on the sky in a standard infrared image acquisition in order to subtract the signal from the Earth's atmosphere from that of Neptune. Because of Neptune's small size relative to the fields-of-view of all of these instruments, images from both chopped positions were recorded on the detector arrays. Additional background stability was established by subtracting an adjacent part of the sky that was similarly chopped. Neptune's small angular size also enabled the telescope displacement for this "nodded"

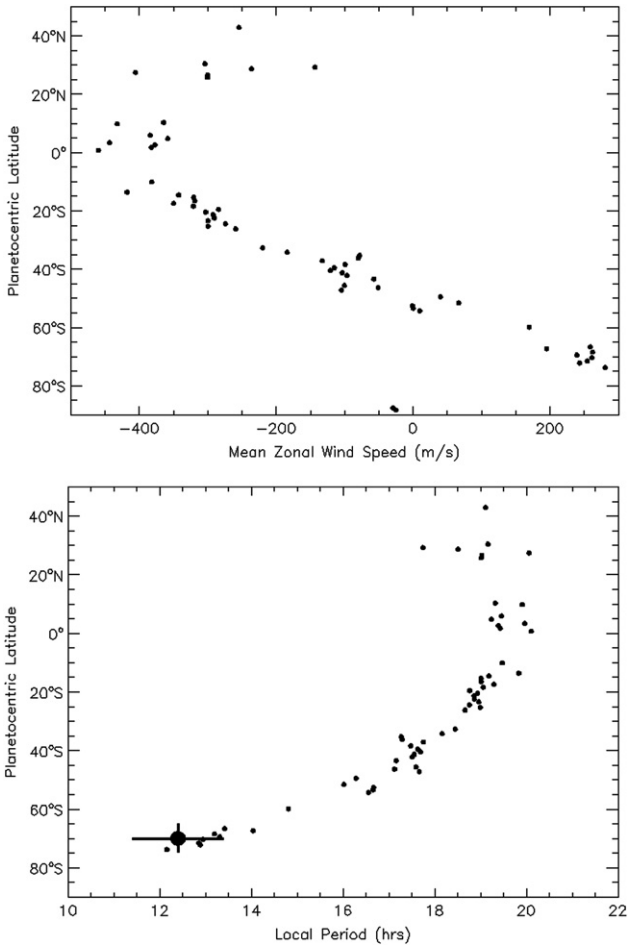

Fig. 3. Top: Mean zonal wind speed of Neptune as a function of latitude derived from Voyager-2 measurements. From Fig. 1A of Sromovsky et al. (1993). Bottom: Rotational period of winds in Neptune as a function of latitude, as derived from the mean zonal wind speeds. The period of the hot spot detected by Orton et al. (2007), 12.4 ± 1.0 h (incorrectly stated originally as 13.9 ± 1.0 h) is denoted by the large filled circle. Uncertainties in latitude arise from the poor spatial resolution near the planetary limb. These winds are relevant to the cloud-top level, estimated as being at the 0.1-bar level by French et al. (1998); they are expected to be weaker (150–200 m s^{-1} near 70°S, see text) at the levels around 1 mbar from which the methane or ethane emission emerges (Orton et al., 2007).

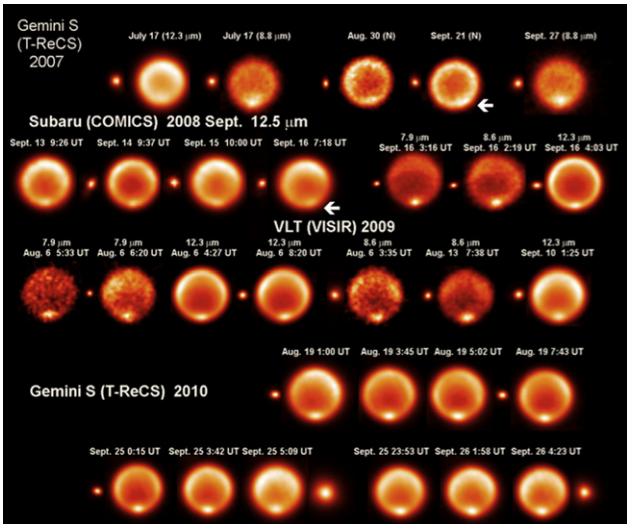

Fig. 4. Images of stratospheric emission from Neptune between 2007 and 2010 from the Gemini South Telescope, the Subaru Telescope and the Very Large Telescope (UT3, "Melipal"). The instrument used is denoted in parentheses. Dates and times at the mid-point of each image acquisition are noted, as is the central wavelength of each filter used, as shown in Fig. 1. Just as in Fig. 2, stellar images obtained close in time to the Neptune images are also displayed in order to characterize the point-spread function: τ Aqr. (HR 8679, HD 216032) for the 2007 Gemini South T-ReCS observations on July 17 and September 17, and 6 Cap. (BS 7754, HD 192947) for the August 30 and September 21 N-band images; π 2 Aqr. (HD 216032) for the Subaru COMICS images on September 13–15 and χ 2 Sgr. (HD 175775); HD 216149 for the 2009 VLT VISIR images on August 6, β Cr.A. (HD 175345) for the August 8 and September 10 images, and θ Psc. (HD 220954) for August 10; 7 Aqr. (HD 199345) for the "early" 2010 Gemini South T-ReCS images and π 2 Aqr. (HD 216032) for the "late" images. Detections of the offset feature are indicated with arrows. Images taken with the broad N-band filter are noisier because they were the result of very short integrations made during the course of acquiring and centering a spectroscopic slit on Neptune's disk. The VLT images in 2008 were acquired serendipitously during the last day of the Subaru observations. The brightness temperatures of the images of ethane emission at 12.3–12.5 μm are close to those of the 2006 images published by Orton et al. (2007), with a maximum radiance corresponding to a brightness temperature of 98–101 K, depending on the quality of the seeing, and a minimum value of 94 K for regions away from the limb. The 8.6–8.8 μm image brightness temperatures are also generally consistent with those of Orton et al. (2007) with a maximum brightness temperature of 108–110 K, again depending on the seeing, with minimum on-disk values of 104 K. The corresponding brightness temperature range for the broad N-band images is 101–105 K, and for the 7.9-μm images it is 120–129 K.

position to be small enough so that the nodded-chopped image set could be recorded on the detector array in almost all cases. This approach yielded four images on the detector array and thus increased the signal-to-noise ratio by a factor of two over a case in which the chopped and nodded positions included only the sky. For the case of COMICS, we followed Subaru standard procedures and used additional sky-only frames to create a correction for the non-uniform response of the detector array. We deemed this unnecessary for the T-ReCS and VISIR data. Several sequences of such chopped and nodded observation sets were incorporated into nearly all the single images shown in Fig. 4. The two exceptions to this were the broad N-band (8–14 μm) filtered images taken to navigate spectral observations (Fig. 4, top row). Co-addition of the images was performed using an autocorrelation approach that was verified in several cases using image-by-image centering and subsequent co-addition. The autocorrelation approach appeared to be robust, except in cases with extraneous emission from bad pixels in what should otherwise be cold sky; in this case, the autocorrelation approach was used with initial guidance to the approximate center of the planet provided manually.

All images were subjected to Wiener filtering, an optimal approach to remove the highest-frequency variations in the image that are indistinguishable from noise. We did not deconvolve any of the images shown in either Figs. 2 or 4. This allows the reader to judge the credibility of the offset detections in the images without the possibility of being compromised by numerical artifacts of the processing. To aid in this judgment, we supply, wherever possible, a nearby stellar image that serves to illustrate the point-spread function characterizing each image in both figures.

The observations were made in filters that were sensitive to stratospheric emission from methane at 7.7 μm, "normal" and deuterated methane at 8.6 μm, and ethane at 12.2 μm. The number of 12.2 μm images of ethane emission dominated our observations, because the radiance at 12.2 μm is much larger than for the shorter wavelengths and an equivalent signal-to-noise ratio could be obtained in a much shorter time. We used nearly all the images we acquired (Fig. 4), despite often non-photometric conditions when images with adequate spatial resolution could be collected. We therefore estimated the radiances for all images based on normalizing the average planetary radiance to the equivalent disk-averaged radiance observed by the Spitzer Infrared

Spectrometer (IRS) instrument, following the same procedure used by Orton et al. (2007).

Although angular resolution is mostly determined by diffraction at these wavelengths, a few images were made in conditions of poor seeing, usually because of high airmass. These were excluded from Fig. 4, except for the 12.3-μm image taken by T-ReCS on 17 July 2007 (Fig. 4, upper left image), which serves to illustrate the best resolution of excluded images. Images at 7.7 and 8.8 μm taken on 10 September 2010 were also excluded because substantial terrestrial water vapor absorption produced images with insufficient signal-to-noise ratios to detect any brightening at the south pole.

Apart from the polar or near-polar hot spot, we note that all the images shown in both Figs. 2 and 4 show evidence for enhanced emissions in the northern hemisphere. This is shown by the enhanced limb brightening in the northern hemisphere in the several images of ethane emission (12.2 or 12.3 μm), some of which show hints of east-west asymmetry. The effect is also present in the 7.9- and 8.6-μm images, as well, in particular the sharp boundary that is most prominent in the VISIR images at 7.9 μm on 16 September 2010. We will examine this asymmetry and its relationship to seasonal vs. dynamical origins in a subsequent paper.

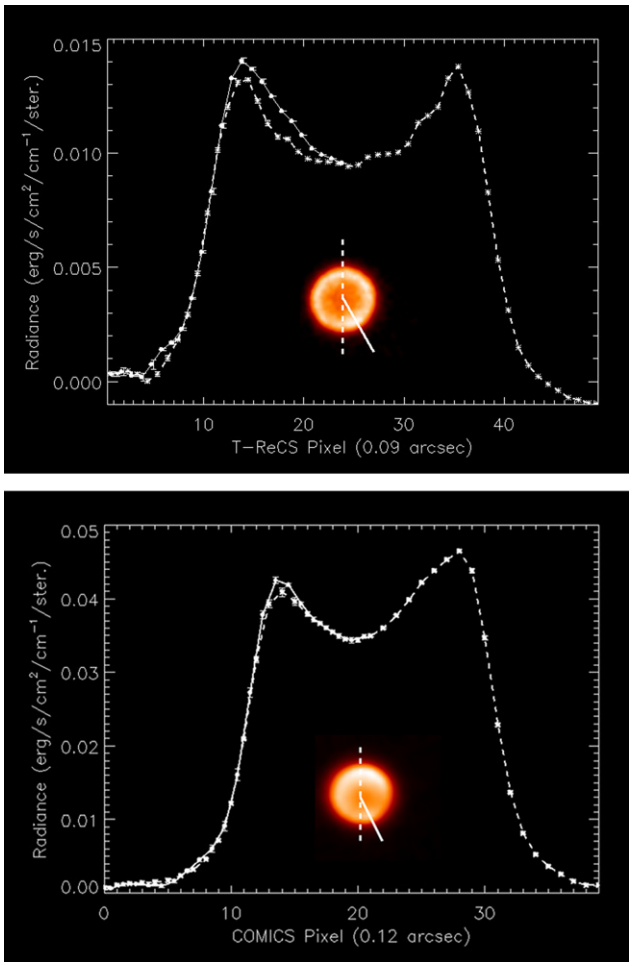

Fig. 5. Plot of cross section of Neptune's brightness vs. position for the two images in which an offset polar hot spot was detected. The top panel shows a plot along the central meridian of the 2007 September 21 T-ReCS N-band image (dashed line). This is compared with a line showing the brightness along a radial line that intersects the center of the offset hot spot (solid line), as illustrated in the inset. The bottom panel shows a similar graph for the 2008 September 16 COMICS 12.5 μm image, with the central meridian (dashed line) and a radial line intersecting the center of the offset hot spot (solid line). Vertical bars denote the error of the mean for each graph, considering a column along the central meridian, together with two adjacent columns, or their equivalent for the offset radial line. In both cases, it is clear that the brightness of the hot spot is higher than a comparable position along the central meridian at or above the 2-standard deviation confidence level.

In our observing proposals, we requested four sets of images over a 7 h interval in which Neptune is available to sample as many longitudes as possible. However, this plan was very often compromised by unfavorable weather, by non-ideal scheduling of some of the observations, or by simply not being granted the full time requested.

Nonetheless, a compact hot feature offset from the pole was detected again at Subaru on 16 September 2008. After this detection, we re-examined our 2007 Gemini data and extended the search to rapid-acquisition images in the broad N-band (Fig. 1) of T-ReCS, which were used to acquire Neptune efficiently for spectroscopic observations. Among those images we detected another instance of an offset feature on 21 September 2007 (Fig. 4 row from the top). Fig. 5 illustrates that in both of these images, the enhancement of radiance in the offset hot spot position over the radiance along the central meridian, the more typical position of a polar hot spot, is significantly higher than the noise level. For both the images, the enhancement in radiance is equivalent to a brightness temperature difference of just over 0.4 K. This is similar to the enhancement typical of the pole over near-polar positions.

Our original observational timing objective was finally met on 19 August 2010 at Gemini South (Fig. 4). Although this was to be followed some two weeks later by a similar set of observations, sufficient to uncouple the cadence of the 12.4 h period of the feature with the Earth's 24 h rotation, inclement weather forced a delay of the observations until September 25, when the fourth observation in the nightly sequence could not be achieved before Neptune had passed hour-angle limits. Although the same sequence was repeated on the subsequent night, the fourth image was obtained at such high airmass that no features were recognizable. Nevertheless, the 2010 observations successfully completed our study of the ephemeral nature of Neptune's off-polar stratospheric hot spot.

3. Discussion

A compact stratospheric hot spot that is near but offset from the pole has now been detected in three out of thirteen epochs of observation, assuming it has a lifetime in excess of 4 days: on 2006 September 2, (Fig. 2), 2007 September 21 and 2008 September 16 (Fig. 4), with a marginal detection on 2005 July 4 (Fig. 2). All detections were consistent with a single feature whose central emission peak is located at planetocentric latitude of 70°S. This assumption groups together the 2008 Subaru and VLT observations in 2008 into a single epoch, together with the 2003 Keck, 2005 Gemini North, 2006 VLT, 2009 August VLT, 2010 August Gemini South and 2010 September Gemini South measurements in distinct epochs. This is only a very rough measure, of course, because it considers equally (i) the several days of observation listed above and (ii) single "snapshots" that covered only a single hemisphere: the Gemini South 30 August, 21 September and 27 September 2007 images, and the VLT 8 August 8, 13 August and 10 September 2009 images. But the 'recovery' of this feature means that we have determined that the phenomenon is not an extremely rare event. This makes it unlikely that the feature detected in 2006 was caused by a single Shoemaker–Levy-like cometary impact, one of the suggestions for its origin made by Orton et al. (2007), despite its consistency with the conjecture by Lellouch et al. (2005, 2010) that the large oxygen content discovered in the form of CO in Neptune's

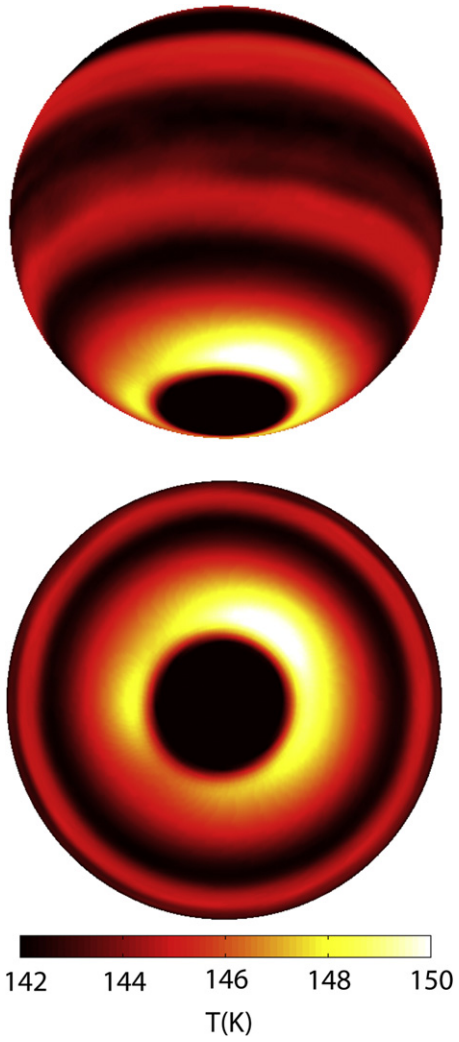

Fig. 6. Top: Orthographic view of the 0.5-mbar temperature structure from a 3D dynamical model of Neptune's upper atmosphere (Liu and Schneider, 2010), as seen from the Earth near the epoch of the 2007–2008 observations, with a peak amplitude of the near-polar wave on the hemisphere facing the Earth. The model lacks seasonally dependent variability, which is why the region closest to the pole is cold. For all the Neptune images in this paper, the south pole has been in sunlight for over 70 years and has subsequently warmed radiatively. The figure has been scaled to display warmer temperatures, which would be prominent in radiances emerging from the atmosphere in the 7–12 μm range. Bottom: Polar view of the same temperature field.

stratosphere could be the product of recent icy impacts. To be caused by multiple impacts, we would need to explain why they were all at near-polar latitudes, which seems extremely unlikely.

An argument for the permanence of the feature in the neutral atmosphere could be based on the 2008 Subaru and VLT observations, again assuming that the feature is not significantly time variable over a 4-day interval. Because the feature emerges from the stratosphere, it is limb brightened and should be detectable over longitudes $\pm 60^\circ$ or more from the central meridian, with limb brightening at high zenith angles, compensated by longitudinal foreshortening close to the limb. Thus, in a longitude system with a 12.4 h period, the sequence of observations in 2008 on September 13–16 from both Subaru and the VLT covered an effective longitude range of 335°, assuming 120° longitude coverage in each of the images shown on these dates in Fig. 4. If the feature were permanent, then coverage of nearly 90% of longitude would have been and, indeed, was sufficient to detect it.

A counter argument would be based on the Gemini South observations in 2010 in which the feature was not detected. Using the same assumptions, the images on August 19 cover nearly 300° of longitude, and those on September 25–26 cover nearly 220° of longitude. The August longitude coverage thus shows that the feature is not present over 83% of the longitudes in a 12.4 h system. If there were no changes in the emission over a nearly 40-day period, then the combined observations in 2010 cover all longitudes in the same system (or systems whose periods range over the 1.0 h uncertainty of this period) and the feature is simply not present. Thus, while a stronger argument could be made with full longitudinal coverage over a short time frame, we assess that it is likely the feature is time dependent.

One of the possible origins of the feature suggested by Orton et al. (2007) was that it might be associated with a perturbation of Neptune's troposphere with a large, buoyant body of warm gas rising rapidly, consistent with the highly variable cloud activity at 70°S latitude, which includes the sudden appearance of broad, singular cloud features (Sromovsky et al., 1993; Rages et al., 2002). Unfortunately, we have been unable to arrange for near-simultaneous supporting observations in the near infrared, so this possibility can neither be verified nor refuted.

We offer an alternative possibility with a physical basis that arises from theoretical considerations and models of atmospheric planetary (Rossby) waves. The feature could be a manifestation of a low-wavenumber (e.g., wavenumber-1) planetary wave whose temperature maximum is detected. Thermal waves are detected in the stratospheres of Jupiter (Magalhaes et al., 1989; Orton et al., 1991) and Saturn (Achterberg and Flasar, 1996; Orton and Yanamandra-Fisher, 2005). Such waves are expected in a stably stratified atmosphere with mean prograde winds in the presence of wave-generating mechanisms such as dynamic instabilities (Andrews et al., 1995). Planetary waves may be generated locally in the stratosphere through barotropic instability; however, given that the zonal wind around 70°S (Conrath et al., 1991; French et al., 1998) is not close to satisfying necessary conditions for barotropic instability, this seems unlikely. Planetary waves may also be generated in the troposphere, for example, by baroclinic instability, which may give rise to the observed cloud activity in Neptune's troposphere around 70°S. Waves generated in the troposphere can propagate upward and become stratospheric waves that are detectable in methane and ethane emission. Because only the longest planetary waves can propagate into the stratosphere ("Charney–Drazin filtering", after Charney and Drazin, 1961), only low-wavenumber features are expected to be detectable in the stratosphere. Planetary wave dynamics would also explain why large wave features are only seen at high latitudes: planetary waves can only propagate where there are mean prograde winds (Andrews et al., 1995). For Neptune (and Uranus), this means they would be confined to higher latitudes, where there is a sufficiently wide latitude range with mean prograde winds to accommodate their meridional excursions which, like their zonal scales, are expected to be large. The meridional excursions in the lobes of the waves may also lead to mixing near the poles, destroying or diminishing the hot spot over the south pole that is visible on Neptune when no hot spot near 70°S is detected (Figs. 2 and 4). In a process dynamically similar to sudden polar warmings in the Earth's winter stratosphere, which occur when planetary waves generated in the troposphere lead to breakup of the winter polar vortex (Andrews et al., 1995), on Neptune this may lead to breakup of a summer polar vortex that confines the polar hot spot, leading to "sudden polar coolings."

Simulations with a 3D general circulation model (GCM) of Neptune's upper atmosphere demonstrate that planetary waves indeed provide an adequate explanation of the observed hot

spots. Fig. 6 shows the temperature at 0.5 mbar at an instant in a Neptune simulation with the model described in Schneider and Liu (2009) and Liu and Schneider (2010). The GCM resolves the flow above the 3-bar level, with implicit links to the (convective) flow and mean meridional circulations at depth and with closed energy and angular momentum budgets that are consistent with observations. In the GCM, the solar radiation is deposited into the atmosphere by scattering and absorption, and the observed intrinsic heat flux is imposed at the lower boundary. This model was not contrived to generate a wavenumber-1 thermal wave at 70°S latitude, the wave appeared as a natural consequence of dynamic instabilities in the model. The wave in the simulation persists over months, with its length scale determined by the zonal flow structure and static stability the model produces. The dissipation of the wave is the result of interactions with the mean flow, which are irreversible on the long radiative timescales of Neptune's stratosphere. The wave in the simulation extends into the deeper atmosphere, but near 100 mbar, the amplitude is fractions of 1 K, which is not detectable above the noise level of our longer wavelength images that are sensitive to this level (Orton et al., 2007).

The interpretation of the thermal hot spot as the warm sector of a (wavenumber-1) planetary wave constrains the phase speed of the wave and the Rossby deformation radius and thus the stratification of Neptune's stratosphere. If the wave is generated in the troposphere and propagates vertically to where it is observed, it needs to obey approximately the inequality

$$0 < \overline{u} - c < \frac{\beta}{n(n+1)/a^2 + (4L_R^2)^{-1}}, \quad (1)$$

where $\overline{u}$ is the mean zonal wind, c is the phase velocity of the wave, β is the planetary vorticity gradient, n is the spherical wavenumber, a is the planet radius and L_R is Rossby radius (Charney and Drazin, 1961). With the planetary vorticity (Coriolis parameter) f and its gradient β evaluated at 70°S and using $L_R = NH/|f| \approx 2100$ km based on a buoyancy frequency $N \approx 1.1 \times 10^{-2}\ s^{-1}$ and scale height $H \approx 40$ km around 1 mbar estimated from the Neptune temperature retrievals in Fletcher et al. (2010), the right-hand side of (1) with $n=1$ evaluates to $\sim 50\ m\ s^{-1}$. This is the maximum phase velocity relative to the mean zonal wind that is possible for a vertically propagating wave. Values for $\bar{u}$ near 1 mbar can be estimated from the thermal wind inferred from Voyager IRIS measurements and flash occultations (Conrath et al., 1991; French et al., 1998); they lie in the range of 150–200 $m\ s^{-1}$ prograde. Barring errors in the temperature retrievals and thus in the estimated Rossby radius, this implies that a vertically propagating wavenumber-1 planetary wave must have a phase velocity exceeding $c \sim 100$–150 $m\ s^{-1}$ but less than $\overline{u}$. Such a phase velocity is near the upper end of but within the uncertainty range of the 12.4 ± 1.0 h rotation periods of the hot spot observed in 2006. The phase velocity, if it can be more precisely measured, may be indicative of the zonal flow in the layers where the wave was generated.

Measuring the phase velocity of the wave thus would provide additional information on Neptune's atmosphere. But this is challenging because it requires a number of observing nights with optimal timing. In addition, Voyager did not provide thermal maps capable of resolving stratospheric winds at these high latitudes, and so measurement of the polar wind speeds from the troposphere are required to answer this definitively. The characterization of tropospheric wave generation mechanisms would be enabled by coordinated near- and mid-infrared imaging. Apart from additional observations, we will pursue adding more physical reality to the dynamical model in the form of seasonal variability, and we will examine the images in quantitative detail to determine, in part, whether there is evidence for suppression of emission over some longitudes that would characterize whether a wavenumber-1 wave as in Fig. 5 is present or whether a higher-wavenumber wave or wave packet is a more accurate description of the phenomenon. The addition of seasonal forcing to the model will also provide the needed context to determine why the pole itself appears colder in the presence of the offset hot region.

Acknowledgements

We thank Erich Karkoschka for helpful comments. Orton and Yanamandra-Fisher conducted a portion of this research at the Jet Propulsion Laboratory, California Institute of Technology, under a contract with NASA. They thank Mark Hofstadter, the Principal Investigator of the relevant program, for this support. De Pater was supported by NSF Grant AST-0908575. Fletcher was supported by a Glasstone Science Fellowship at the University of Oxford. Schneider and Liu acknowledge support by a David and Lucile Packard Fellowship and by the NASA Outer Planets Research Program (Grant NNX10AQ05G). Fujiyoshi and Fuse were supported by the National Astronomical Observatory of Japan. Edwards and Geballe were supported by the Gemini Observatory, on behalf of the Gemini partnership: the National Science Foundation (United States), the Science and Technology Facilities Council (United Kingdom), the National Research Council (Canada), CONICYT (Chile), the Australian Research Council (Australia), Ministrio da Cinica e Tecnologia (Brazil) and Ministerio de Cienica, Tecnologia e Innovacin Productiva (Argentina). The simulations on which Fig. 5 is based were performed on Caltech's Division of Geological and Planetary Sciences Dell cluster.

The new results presented in this paper were based, in part, on observations made at the European Southern Observatory telescopes, in programs 081C-0496(A) and 083C-0163(A) and (B), obtained from the ESO/ST-ECF Science Archive Facility; on data collected at Subaru Telescope in program ID S08-032, which is operated by the National Astronomical Observatory of Japan; and on data obtained from the Gemini North Telescope in program GN-2007B-A-105 and the Gemini South Telescope in programs GS-2007B-Q-47, GS-2010B-A-42, which are operated by the Association of Universities for Research in Astronomy.

References

Achterberg, R.K., Flasar, F.M., 1996. Planetary scale waves in Saturn's upper troposphere. Icarus 119, 350–369.

Andrews, D.G., Holton, J.R., Leovy, C.B., 1995. Middle Atmosphere Dynamics. Academic Press.

Charney, J.G., Drazin, P.G., 1961. Propagation of planetary-scale disturbances from the lower into the upper atmosphere. J. Geophys. Res. 66, 83–109.

Conrath, B.J, Flasar, F.M, Gierasch, P.J., 1991. Thermal structure and dynamics of Neptune's atmosphere from Voyager measurements. J. Geophys. Res. 96, 18931–18939.

de Buizer, J., Fisher, R., 2005. T-ReCS and Michelle: The Mid-Infrared Spectroscopic Capabilities of the Gemini Observatory. In: Kaufl, H.U., Siebenmorgen, R., Moorwood, A. (Eds.), High Resolution Infrared Spectroscopy in Astronomy, pp. 84–87.

Fletcher, L.N, Irwin, P.G.J., Orton, G.S., Teanby, N.A., Achterberg, R.K., Bjoraker, G.L., Read, P.L., Simon-Miller, A.A., Howett, C., de Kok, R., Bowles, N., Culcutt, S.B., Hesman, B., Flasar, F.M., 2008. Temperature and composition of Saturn's polar hot spots and hexagon. Science 319, 79–81.

Fletcher, L.N., Drossart, P., Burgdorf, M., Orton, G.S., Encrenaz, T., 2010. Neptune's atmospheric composition from AKARI infrared spectroscopy. Astron. Astrophys. 514, A17.

French, R.G., McGhee, C.A., Sicardy, B., 1998. Neptune's stratospheric winds from three central flash occultations. Icarus 136, 27–49.

Gillett, F.C., Orton, G.S., 1975. Center-to-limb observations of Saturn in the thermal infrared. Astrophys. J. 195, L47–L49.

Hammel, H.B., Sitko, M.L., Lynch, D.K., Orton, G.S., Rusell, R.W., Geballe, T.R., de Pater, I., 2007. Distribution of ethane and methane emission on Neptune. Astron. J. 134, 637–641.

Kataza, H., Okamoto, Y., Takubo, S., Onaka, T., Sako, S., Nakamura, K., Miyata, T., Tamashita, T., 2000. COMICS: the cooled mid-infrared camera and spectrometer for the Subaru Telescope. Proc. SPIE 4008, 1144–1152.

Lagage, P.-O., Durand, G.A., Lyraud, C., Rio, Y., Pel, J.-W., de Haas, J.C., 2000. Final design of VISIR: the mid-infrared imager and spectrometer for the VLT. Proc. SPIE 4008, 1120–1131.

Lellouch, E., Moreno, R., Paubert, G., 2005. A dual origin for Neptune's carbon monoxide? Astron. Astrophys. 430, L37–L40.

Lellouch, E., 53 co-authors, 2010. First results of Herschel-PACS observations of Neptune. Astron. Astrophys. 518, 152L.

Liu, J., Schneider, T., 2010. Mechanisms of jet formation on the giant planets. J. Atmos. Sci. 67, 3652–3672.

Magalhaes, J.A., Weir, A.L., Conrath, B.J., Gierasch, P.J., Leroy, S.S., 1989. Slowly moving thermal features on Jupiter. Nature 337, 444–447.

Martin, S., de Pater, I., Kloosterman, J., Gibbard, S., Hammel, H.B., 2006. Multi wavelength imaging of Neptune at high spectral resolution. Bull. Am. Astron. Soc. 38, 502.

Martin, S., de Pater, I., Kloosterman, J Hammel, H. B. 2008. Multi-wavelength observations of Neptune's atmosphere. EPSC Abstracts vol 3, EPSC2008-A-00277.

Orton, G.S., Friedson, A.J., Caldwell, J., Hammel, H.B., Baines, K.H., Bergstralh, J.T., Martin, T.Z., Malcom, M.E., West, R.A., Tokunaga, A. .T., Griep, D.M., Golisch, W.F., Kaminsky, C.D., Barons, R, Am, Shure, 1991. Thermal maps of Jupiter: spatial organization and time dependence of stratospheric temperatures, 1980-1991. Science 252, 537–542.

Orton, G.S., Yanamandra-Fisher, P.A., 2005. Saturn's temperature field from high-resolution middle-infrared imaging. Science 307, 696–701.

Orton, G.S., Encrenaz, T., Leyrat, C., Puetter, R., Friedson, A.J., 2007. Evidence for methane escape and strong seasonal and dynamical perturbations of Neptune's atmospheric temperatures. Astron. Astrophys. 473, L5–L8.

Rages, K., Hammel, H.B., Lockwood, G.W., 2002. A prominent apparition of Neptune's south polar feature. Icarus 159, 262–265.

Schneider, T., Liu, J., 2009. Formation of jets and equatorial superrotation on Jupiter. J. Atmos. Sci. 66, 579–601.

Sromovsky, L.A., Limaye, S.S., Fry, P.M., 1993. Dynamics of Neptune's major cloud features. Icarus 105, 140–141.

Telesco, C.M., Pina, R.K., Hanna, K.T., Julian, J.A., Hon, D.B., Kisko, T.M., 1998. GatirCam: Gemini mid-infrared imager. Proc. SPIE 3354, 534–544.